Proceedings of the 6th International Conference on Gas Hydrates (ICGH 2008),
Vancouver, British Columbia, CANADA, July 6-10, 2008.

GRAIN SCALE STUDY OF HYDRATE FORMATION IN SEDIMENTS FROM METHANE GAS: ROLE OF CAPILLARITY

Javad Behseresht, Yao Peng, Maša Prodanović, Steven L. Bryant*
Department of Petroleum and Geosystems Engineering
The University of Texas at Austin
1 University Station C0300, Austin, TX, 78712-0228
USA

ABSTRACT

Ocean sediments bearing methane hydrates exhibit a range of behavior, from cold seeps where solid and gas phases coexist in the hydrate stability zone (HSZ), to essentially static accumulations where solid and liquid co-exist. This and the companion paper by Jain and Juanes [1] describe the development and application of models for grain-scale phenomena governing in situ gas-to-hydrate conversion. The motivation is the following hypothesis: as gas phase pore pressure varies, the competition between brine displacement and sediment fracturing determines the extent of conversion of methane gas entering the HSZ to hydrate. Here we implement the level set method to determine the capillarity-controlled displacement of brine by gas from sediment and from fractures within the sediment. Reduction of gas phase pressure, for example due to disconnection from the source gas accumulation, allows imbibition to occur. Drainage into infinite-acting model sediments indicate that the brine in drained sediment (after invasion by methane gas) is better connected than previously believed, thus facilitating hydrate formation within sediment. Nevertheless drainage to the endpoint condition of irreducible brine saturation is unlikely to account for co-existence of free gas and hydrate because it implies a large free gas saturation, which is not observed. Nor does the large gas saturation at the drainage endpoint lead to large hydrate saturations such as those reported for the Mallik well, because insufficient water is present and the requisite water can only enter the sediment by imbibition. Several drainage/imbibition cycles would be needed instead. Work is underway (see companion paper [1]) to couple this capillarity-controlled displacement model with a discrete element model for grain-scale mechanics. Here we present a simple kinematic version of this coupling. The qualitative effect is to lower the percolation threshold and to increase irreducible water saturation. This would diffuse the propagation of a fracture into the surrounding sediment and reduce the free gas saturation preceding hydrate formation, but the conditions leading to gas phase and hydrate coexistence cannot be readily ascertained.

Keywords: gas hydrates, capillarity, drainage, imbibition, interfacial area

NOMENCLATURE

a_0	prescribed pressure-like coefficient in speed function , Eqs. (3) and (4), L/t
b_0	prescribed interfacial-tension like coefficient in speed function , Eqs. (3) and (4), L^2/t
C	normalized critical curvature estimate by Mason and Mellor

* Corresponding author: Phone: +1 512 471 3250 Fax +1 512 471 9605 E-mail: steven_bryant@mail.utexas.edu

C_i	twice the mean curvature at step i of the PQS algorithm, L^{-1}
dx	grid spacing (numerical simulations), L
$\vec{d_i}$	displacement of grain i
F	speed of interface in level set method evolution equation, Eq. (2), L/t
$\vec{F_i}$	force exerted by non-wetting fluid in grain I, ML/t^2
K	pseudo-bulk modulus for nonwetting phase
P_c	capillary pressure, $M/L/t^2$
R_{avg}	average sphere radius in a packing, L
$r_{inscribed}$	throat inscribed sphere radius, L
S_i	saturation of phase i
$V(t)$	volume of nonwetting phase at time t, L^3
V_m	prescribed target volume of nonwetting phase, L^3
$\vec{x}$	coordinates of a point in space
ϕ	level set function
κ	twice the mean curvature, L^{-1}
ψ	level set function for imposing mask corresponding to void/solid boundary

INTRODUCTION

Estimates of the mass of methane hydrate in ocean sediments and in permafrost regions vary widely. Contributing to the variability is the difficulty in determining the growth habit and the spatial distribution of hydrate within the hydrate stability zone (HSZ). The mode in which methane is transported in the HSZ presumably affects the spatial distribution of hydrate. This is our motivation for developing a predictive, mechanistic model of transport. The contribution of capillarity-controlled fluid displacement to transport is the focus of this paper.

Because gas, water and hydrate phases are frequently (though not universally) observed to co-exist within the HSZ, we focus on the phenomena associated with two-phase flow. One key phenomenon is capillarity: if gas phase pressure exceeds water phase pressure by an amount sufficient to force the gas/water meniscus into a critical fraction of pore throats, then the gas phase can drain water from the sediment. The other key phenomenon is grain-scale mechanics: if the gas phase pressure exceeds any of the principal stresses confining the sediment, then the gas phase can fracture the sediment. The geometry of the invaded region is quite different for each phenomenon.

Since drainage and fracture initiation each require a different threshold pressure to be exceeded, we anticipate that one or the other phenomenon will be dominant in a given situation. However, some coupling between these mechanisms is also possible. For example, a fracture may propagate vertically into a region of coarser-grained sediment where the threshold pressure for drainage is smaller. The capillarity-driven invasion of gas phase laterally into this sediment could halt the fracture propagation. On the other hand, fracturing rearranges sediment grains in the vicinity of the fracture face. This is likely to reduce the size of pore throats near the face, thereby increasing the threshold for subsequent drainage. The grain rearrangement will also change the manner in which water imbibes into the fracture, should the gas pressure be reduced later.

In this paper we describe mechanistic grain-scale models for the capillarity-controlled displacement of brine by gas. We extend the model to account heuristically for displacement of sediment grains by the pressure imbalance between gas and water phases. The implications of model predictions for water and gas availability for hydrate formation are discussed.

MODELING APPROACH

Geometric Models of Sediments

To obtain simple but realistic models of pore space in sediments, we construct densely packed, randomly arranged spheres with prescribed distributions of radii using a cooperative rearrangement algorithm [2]. The spatial coordinates and radius of each sphere are known. The spheres are packed in a periodic unit cell to eliminate edge effects. Knowledge of the sphere centers permits subdividing the pore space into uniquely defined pore bodies by Delaunay tessellation [3,4]. The tessellation yields a set of tetrahedra whose vertices are the coordinates of the sphere centers. The faces of a tetrahedron correspond to pore throats, because these locally narrowest constrictions control access of the gas/water meniscus during drainage.

Network Model of Drainage of Model Sediment

The details of our drainage simulation have been given in [5,6] Here we present an overview of the approach.

A simulation of drainage in a model sediment requires knowledge of the critical curvature in each pore throat in the sediment. This is the

meniscus curvature (equivalently, the capillary pressure) at which the meniscus just passes through a pore throat. We show below that the estimate of critical curvature proposed by Mason and Mellor [7] is reasonably accurate for the model sediments considered here:

$$C = \frac{2R_{avg}}{r_{inscribed}} - 1.6 \quad (1)$$

In the above equation, R_{avg} is the average sphere radius in the model sediment, and $r_{inscribed}$ is the radius of the inscribed sphere in a throat. We also employ the Mayer-Stowe-Princen estimate [8-11].

Many (but not all) pairs of neighboring grains in a sediment are in contact. After pores surrounding a grain contact have drained, wetting phase is held as a pendular ring at the contact. Narrow gaps separate some pairs of grains, which can support a liquid bridge of wetting phase after nearby pores have drained. These rings and liquid bridges have small volumes, but they play an important role in connecting not-yet-drained pores.

From the known sphere locations in the periodic model sediments, we extract a network of pores that is also periodic. The periodicity is guaranteed by the Delaunay tessellation used to define the network and the periodicity of the packing, but it is not trivial, because the sphere locations are random. These networks can be regarded as "infinite-acting" because there is no natural choice of "outlet pores" for the displaced water phase. We adopt the concept of a percolating cluster of pores to replace the notion of outlets. We simulate drainage with a standard invasion percolation algorithm, modified to allow for trapping of wetting phase. The simulation starts with the pore space full of wetting phase.

Wetting Phase Trapping

Displacing a fluid from a pore presumes that fluid can be accommodated elsewhere. In a traditional finite network, "elsewhere" means an exit from the network. The infinite-acting networks used here have no true boundaries and thus no exit pores. Instead we treat wetting phase as displaceable if the pore containing it is member of any periodically connected cluster of pores. Such a cluster "wraps around" the faces of the periodic network to connect to itself. This loop approximates a percolating (infinite) cluster of pores occupied by wetting phase. All other wetting phase is considered trapped.

Wetting Phase Connectivity

To determine whether pores containing wetting phase are members of a cluster, a criterion for "connected" is needed. Traditional networks consider pores to be connected only via pore throats. In sediments, the wetting phase also exists as partially-formed pendular rings at grain contacts. Partial rings are created when some, but not all, pores associated with the grain contact have drained. The partial rings can connect wetting phase in nearby pores even if those pores do not share a throat. Accounting for these connections is important; without them simulations overestimate typical experimental irreducible wetting phase saturations [5].

Level Set Method (LSM) for Interface Tracking: the Progressive Quasi-Static (PQS) Algorithm

Assuming slow changes in capillary pressure, immiscible displacement can be modeled as a quasi-static, capillarity-controlled process. Thus tracking fluid interfaces at each stage of displacement is equivalent to finding constant mean curvature (κ_M) surfaces, satisfying Young-Laplace equation $P_c = P_{nw} - P_w = 2\sigma\kappa_M = \sigma\kappa$ where nw and w denote non-wetting and wetting phases respectively, P_c is capillary pressure and σ is interfacial tension. Presently we assume perfectly wetted grains, so that the contact angle is zero.

In [12-14] we described a simple but robust model for simulating both drainage and imbibition in general porous media assuming capillary forces are dominant. The method is robust with respect to porous medium geometry and can be used to simulate displacement in individual pores and throats as well as in the arbitrary rectangular subvolume.

We describe the method briefly, and refer the reader to [12, 13] for more details. In level set methods the interface of interest is embedded as a zero level set of a function described on entire domain, $\varphi(\vec{x}, t) = 0$. The interface evolution is then given by the following equation

$$\varphi_t + F|\nabla\varphi| = 0 \quad (2)$$

where $F(\vec{x},t)$ is the speed of the interface in the normal direction (given by the physics of the problem). In our case, this speed will come from Young-Laplace equation as detailed below.

We start drainage simulations by placing a planar or circular interface near the entry of the computational domain. The interface is propagated with the slightly compressible velocity model, which defines the speed F as

$$F(\vec{x},t) = a_0 exp[K(1 - \frac{V(t)}{V_m})] - b_0\kappa(\vec{x},t) \quad (3)$$

The first term on the right hand side behaves like a capillary pressure, with prescribed pressure value a_0, target volume V_m and bulk-modulus K, and $V(t)$ is the non-wetting phase volume. The second term represents surface energy density, with b_0 corresponding to interfacial tension, and $\kappa(\vec{x},t)$ is (twice) the mean curvature. With this speed function we integrate Eq. (2) in time until a steady state ϕ_I with the corresponding pressure a_I is reached. At steady state, the speed F is everywhere zero. Eq. (3) shows that the physical situation at steady state corresponds to a balance between capillary pressure and interfacial tension, i.e. the Young-Laplace equation. Note that the time is not a physical parameter as we only seek steady state solution of Eq. (2).

At each further step in drainage we increase curvature by $\Delta\kappa$ (which is equivalent to incrementing capillary pressure by $\Delta a = b_0\Delta\kappa$), and run the prescribed curvature model

$$F(\vec{x},t) = a_0 - b_0\kappa(\vec{x},t) \quad (4)$$

until a new steady state is obtained, representing a balance between capillary forces and pressure forces. After each step of this quasi-static model, volume of the fluid, interfacial areas of interest, number of disconnected fluid components as well as any topological changes are easily computed. Such changes might indicate some critical pore level events such as Haines jumps in throats during drainage or imbibition of a (set of) pore(s).

There is an inexpensive numerical boundary condition that prevents the interface from entering grain space and results in a zero contact angle: we impose $\phi(\vec{x},t) \leq \psi(\vec{x})$ after every iteration, where ψ is a fixed level set function whose zero level set is pore-grain boundary surface. Level Set Method Library [15] contains most of the routines required for implementation in C/C++/FORTRAN. Please see [12, 14] for more implementation details.

PQS Fluid Displacement Coupled with Grain Displacement

Detailed knowledge of both fluid-fluid and fluid-solid interfaces from PQS algorithm, as well as the geometry of each individual grain, allows us to isolate individual fluid-solid contacts. As a means of exploring the coupled behavior of meniscus movement and grain movement, we develop an approach with simplified kinematics rules for grain displacement, and accurately computed fluid-fluid interface. The following grain displacement steps are introduced after each PQS drainage step:

1) Find grains in contact with non-wetting phase.
2) The non-wetting fluid (gas) exerts force, the vector sum of which we denote $\vec{F_i}$, on each grain i found in step 1. As in the elastic membrane model, the force is locally normal to the fluid-grain contact (see Figure 1). Thus to obtain $\vec{F_i}$, we integrate the normal vector $\vec{n}$ (pointing outwards from the gas phase) along the part Γ_{Gi} of the entire grain perimeter (surface) Γ_i in contact with gas. Finally, we find the unit vector $\vec{f_i}$ in the same direction as $\vec{F_i}$.
3) Compute a displacement $\vec{d_i}$ in response to the force computed in step 2. The force is maximum when Γ_{Gi} is half-circle (half-sphere) so we set $\vec{d_i} = 4r(1-r)k_0\vec{f_i}$, where r is ratio of the lengths (areas) of Γ_{Gi} and of entire Γ_i, and k_0 is a pre-set constant.
4) The center of grain i moves by $\vec{d_i}$ determined in step 3, but only if it will not overlap substantially with any other grains in its new position. Definition of substantial overlap is somewhat arbitrary and in this work we require that the distance between the grain centers would be less than 0.8 of the sum of their respective radii.

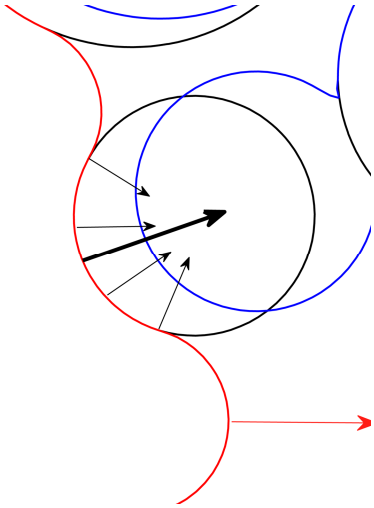

Figure 1. Sediment movement in case of two grains (this is isolated from the simulation show later in Results section, see Figures 6-8). Non-wetting fluid (gas) interface is shown in red and the initial grain position is shown in black. Small black arrows indicate some of the normal vectors along the on-wetting fluid-grain contact line and enlarged black arrows show their (integral) direction (and ultimately direction of the movement). New grain positions are outlined in blue.

This conceptual procedure does not consider the forces imposed by neighboring grains, which are the essence of the solid mechanics; this is the proper role of discrete element method (DEM) described in the companion paper [1]. Thus we do not attempt to determine the exact magnitude of F_i, nor the exact displacement $\vec{d_i}$ from Newton's 2nd law. The kinematic approach simply provides insight into the type of behavior that can arise from the coupled displacements.

RESULTS

LSM/PQS has been shown to accurately predict critical curvature for drainage [12]. Results shown in Figures 2 and 3 for two different packings indicate that the Mason/Mellor semi-empirical estimate is also reasonable for many throats in a polydisperse packing (the estimate was postulated only for monodisperse packings). This is convenient since the latter is easily calculated. The more rigorous Mayer-Stowe-Princen estimate is much more complicated to compute for grains of different sizes.

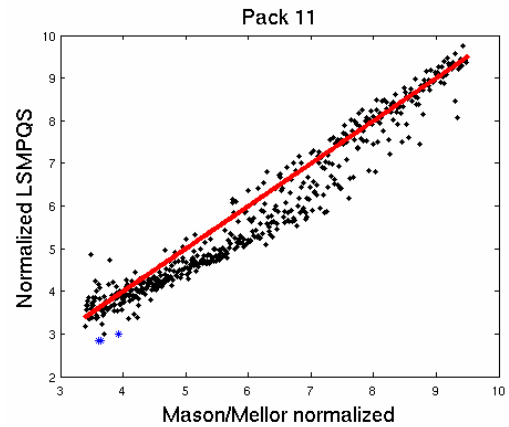

Figure 2. Critical curvatures estimated by the LSMPQS algorithm vs. the Mason and Mellor estimate (Eq. (1)). Black points show the results for 500 throats from Pack 11 whose normalized inscribed radius ($r_{inscribed}/R_{avg}$) lies in [0.1,0.4].

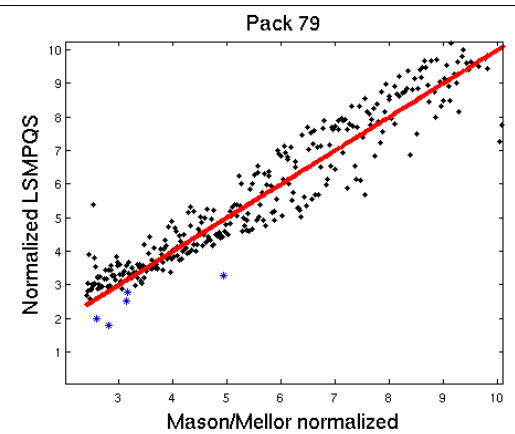

Figure 3. Critical curvatures estimated by the LSMPQS algorithm vs. the Mason and Mellor estimate (Eq. (1)). Black points show the results for 500 throats from Pack 79 whose normalized inscribed radius ($r_{inscribed}/R_{avg}$) lies in [0.1,0.4].

Drainage in Model Sediments

Using the Mayer-Stowe-Princen estimate of critical curvature and the infinite-acting networks, we simulate drainage in several model sediments having different sorting. One packing is monodisperse (porosity = 36%). The others have normal grain size distributions with means and standard deviations given in Table 1. The drainage curves (Figure 4) are presented as curvature normalized by the mean grain radius vs. brine saturation. The entry pressure decreases for the packing with the widest grain size distribution, but the irreducible water saturations are the same for all packings. In all cases the percolation threshold

is sharp: a small increase in capillary pressure above the entry value causes a large decrease in wetting phase saturation. The absence of a steep "tail" near irreducible water saturation is due to the percolating cluster requirement for wetting phase displacement.

Packing Number	Mean Radius	Standard Deviation	Porosity
11	2.12	0.43	0.34
41	2.17	0.07	0.38
49	2.01	0.67	0.34
53	1.86	0.89	0.35
79	1.93	0.89	0.34

Table 1. Summary of Properties of Different Packings

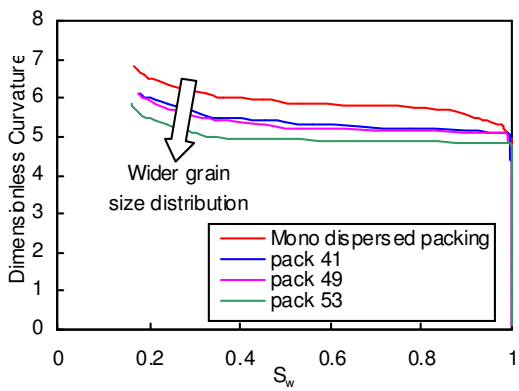

Figure 4. Drainage curves in infinite-acting networks for a selected number of sphere packings.

Disconnection and Trapping of Wetting Phase

We track the disconnection of wetting phase during drainage according to the trapping criteria described above. The wetting phase remains very well connected even after 50% of the pore volume has been invaded by the gas phase. But as drainage reduces the wetting phase saturation below 30%, the saturation of trapped wetting phase increases rapidly. Figure 5 illustrates this behavior for the monodisperse model sediment.

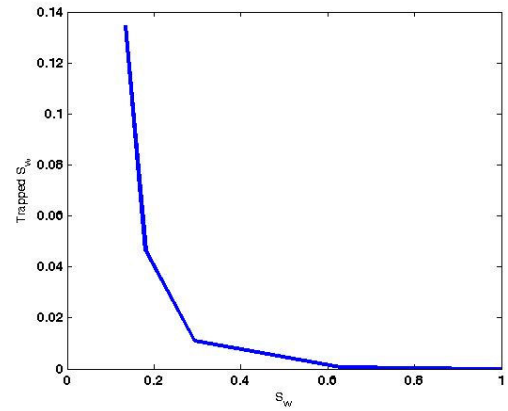

Figure 5. During the early stages of drainage (S_w decreases to 0.6 from 1) of a model sediment of equal spheres, the trapped wetting phase saturation is extremely small. Disconnection of isolated pores of wetting phase begins as S_w decreases between 0.6 and 0.4. Disconnection becomes rapid for S_w below 0.3; at the endpoint of irreducible saturation, all the wetting phase remaining in the pore space is trapped.

Effect of Movable Grains on DRAINAGE CURVE

We illustrate coupling LSM/PQS drainage simulation with simple grain kinematics in a 2D pack of circular grains. We obtained the pack by taking a cross-section of packing 11, resulting in disks with radii values in [0.2,3.6], and discretized it using grid spacing $dx = 0.08$. The starting fluid configuration is shown in Figure 6. Figures 7 and 8 show fluid configurations at selected curvatures with and without grain displacement. Corresponding drainage curves are shown in Figure 9.

When fluid pressure displaces the grains the domain begins to drain at smaller curvatures. This makes intuitive sense: moving grains apart decreases the critical curvature required to force a meniscus between them. Less obvious is the second observation. Behind the advancing gas phase, grains are pushed into each other, narrowing the pore throats between them. This increases the pressure required to invade the undrained region behind the leading edge of the advancing front. Thus the drainage curve is smoothed out in the coupled displacement. Moreover the displacement leads to clustering of grains around pockets of trapped wetting phase. These kinematic simulations show little quantitative difference, but we expect these

clusters to yields larger irreducible water saturations than in fixed-grain drainage. In some cases [6] the drainage curve becomes steeper as well.

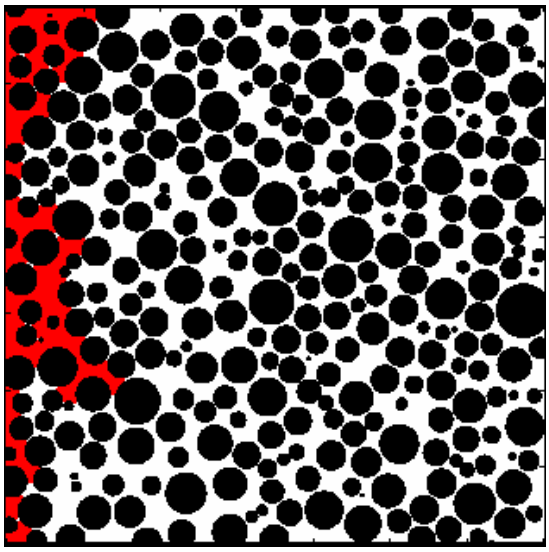

Figure 6. Fluid configuration at $C_1 = 2.12$ (result of slightly compressible model) for drainage simulation (with or without coupling with grain mechanics). Grains are shown in black, non-wetting fluid in red and the wetting fluid in the rest of the pore space is in white.

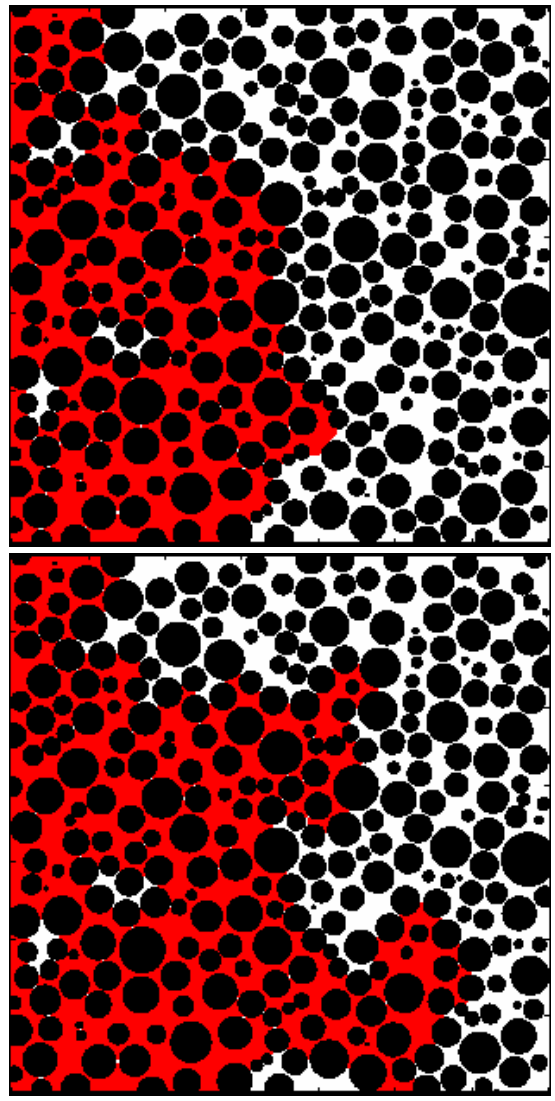

Figure 7. Fluid configuration at steps $C_5 = 2.92$ and $C_6 = 3.12$ for drainage with stationary grains. Grains are shown in black, non-wetting fluid in red and the wetting fluid in the rest of the pore space is in white.

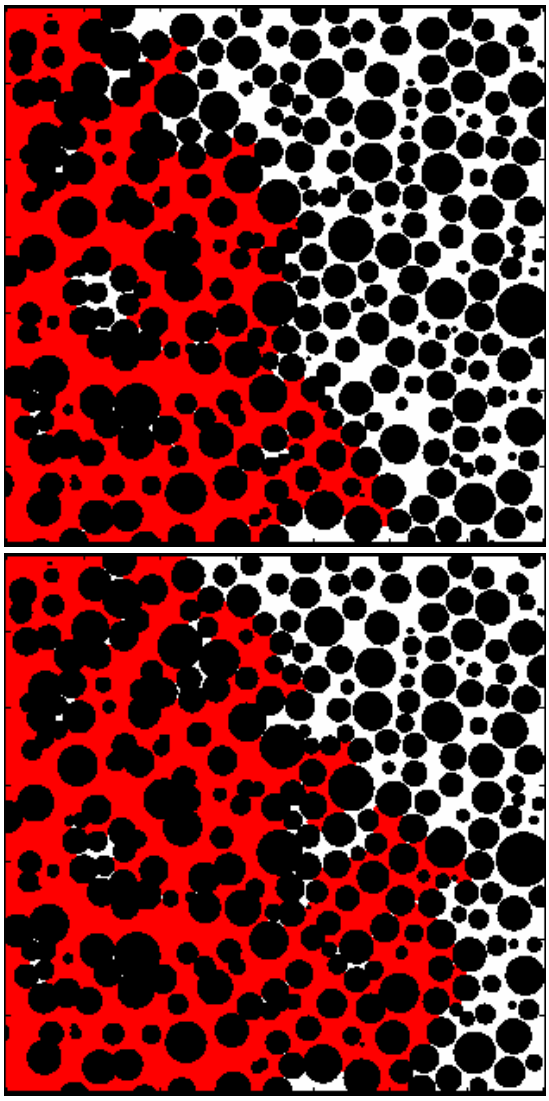

Figure 8. Fluid configuration for drainage coupled with grain mechanics, steps $C_4 = 2.82$ and $C_5 = 2.92$. Grains are shown in black, non-wetting fluid in red and the wetting fluid in the rest of the pore space is in white.

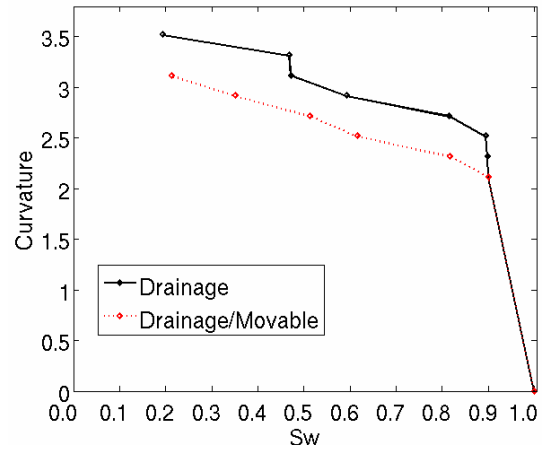

Figure 9. Curvature-wetting fluid saturation curves corresponding to drainage simulations with and without coupling with grain displacement.

DISCUSSION

We now turn to the growth habit of methane hydrate, assuming hydrate forms after comparatively rapid drainage of a sediment. A consistent feature of the drainage curves in the fixed-grain sediments, Figure 4, is a rather sharp percolation threshold. That is, once gas reaches a critical capillary pressure in these well-sorted sediments, a large change in saturation occurs with a comparatively small increment in pressure. Thus in practice it is likely that drainage will proceed to the endpoint of irreducible brine saturation.

Hydrate Formation from Drainage Endpoint in Well-sorted Fixed-grain Sediment

The water comprising the irreducible saturation is disconnected from the bulk brine phase. Typical values of S_{wirr} expected in natural sediments are 20% (smaller values are observed in the laboratory because the sample has exit pores, which permit water displacement even after a percolating cluster is disconnected [5]). Much of it occurs as isolated clusters of one or two pores and as pendular rings, but there are also a few clusters of several hundred to several thousand pores. Because it is disconnected and because its saturation is relatively small at the drainage endpoint, water is the limiting reactant under typical conditions in the HSZ. Thus we expect gradual conversion of water to hydrate in these trapped clusters until the increasing salinity in the remaining water in a cluster makes the hydrate unstable at the prevailing temperature and pressure.

In the hypothetical limit of complete water conversion, the resulting hydrate saturation (volume fraction of pore space occupied) would be about 27% (we assume a stoichiometry of six H_2O to one CH_4 in the hydrate and a hydrate density of 900 kg/m^3). This would be an upper limit, since there is no pathway for transporting dissolved ions out of the disconnected volumes of water. The hydrate would be distributed uniformly through the sediment (at every grain contact, in many small pores, in a few extensive clusters). The assumption of fixed grains means the sediment matrix would appear intact, unfractured by gas pressure or by freezing.

At all stages of drainage the gas phase is completely connected. Thus it would be possible to transport the methane needed to maintain the gas phase pressure as the formation of hydrate consumes the methane that originally drained into the sediment. A large gas phase saturation (~75%) would exist after hydrate formation was complete. This is qualitatively consistent with observations of co-existing gas, hydrate and brine, e.g. at Hydrate Ridge [16, 17], at Green Canyon in the Gulf of Mexico [18] and the Gulf of Guinea [19]. However, quantitative assessment at Hydrate Ridge [20] indicates a 10% saturation of free gas and 50% saturation of brine. The free gas saturation is estimated to be 1% in the Gulf of Guinea. Drainage to irreducible brine saturation of a moderately well sorted fixed-grain sediment evidently cannot explain these observations.

Collett *et al*. [21] infer hydrate saturations of 60% to 80% in several intervals penetrated by the Mallik research well. Much of the sediment containing hydrate in this well is reasonably approximated by the sphere pack models we use here. However it is not possible to obtain such large saturations from a drainage endpoint. Imbibition of water into the drained sediment would have to occur to meet the stoichiometric requirement of converting the gas to hydrate. Imbibition requires the gas phase pressure to decrease. This could occur if pressure were to decrease in the methane source (e.g. a gas accumulation below the HSZ) as it is depleted. If gas drains into a sediment from a fracture, the pressure could decrease as the fracture continues to propagate upwards. In either case, reconnecting the water phase in the sediment would enable transport of dissolved ions out of the sediment, enabling continued conversion.

We will report the implications of a mechanistic imbibition simulation for hydrate growth habit in future work. Here we remark that a mechanistic model in similar model sediments using the Melrose criterion of imbibition [22], predicts residual saturations of methane to be distributed in many small pores and a few large clusters, at a saturation of 15%. At the Mallik well conditions, the complete conversion of this trapped methane to hydrate would yield a hydrate saturation of about 11%. The total hydrate saturation (formed at drainage endpoint, then formed at imbibition endpoint) would be 38%. These considerations indicate that if capillarity controls interface movement, forming a hydrate saturation of 60% or more would require either a series of drainage/imbibition cycles, or a mechanism that prevents gas invasion from proceeding to the drainage endpoint.

Hydrate Formation After Drainage in Movable-grain Sediment

When the sediment grains can be moved by the higher pressure in the gas phase, drainage tends to trap water in larger clusters and to increase irreducible water saturation. In some cases the drainage curve becomes steeper, with greater increments in capillary pressure needed to displace the same saturation of water. This raises the possibility that drainage need not proceed all the way to the irreducible wetting phase saturation endpoint. Indeed, to reach the endpoint, gas phase pressure would have to build up to a value considerably larger than the threshold for initiation of drainage. This is conceivable for drainage from a gas-driven fracture propagating into a coarser sediment. But in most situations it is likely that the grain movement would result in drainage to an intermediate water saturation.

In fixed-grain drainage simulations, the wetting phase remains very well connected until close to the drainage endpoint. If this holds true in movable-grain sediments, then after drainage to an intermediate saturation neither the supply of methane nor the supply of water would impose an immediate restriction on the growth of hydrate. Thus in contrast to the drainage endpoint, a spectrum of behavior is possible. The ultimate achievable hydrate saturation and the possibility of

a free gas phase remaining would depend on the details of hydrate growth from the gas/water interface and the pressure history in the gas phase.

We emphasize that the movable-grain model presented here is qualitative. The degree to which grains can be moved and the competition between fracture propagation and drainage require a fully mechanistic, coupled 3D model. Behseresht *et al*. [6] and the companion to this paper [1] presented a methodology for such coupling. We plan to present results from that effort in future publications.

ACKNOWLEDGEMENTS

This work was supported by the Department of Energy DE-FC26-06NT42958.

REFERENCES

[1] Jain, A.K. and R. Juanes. Pore scale mechanistic study of the preferential mode of hydrate formation in sediments: Coupling of fluid flow and sediment mechanics. Presented at ICGH Conference, Vancouver, British Columbia, Canada, July 6-10, 2008

[2] Thane, C.G. Geometry and Topology of Model Sediments and Their influence on Sediment Properties. Department of Petroleum and Geosystems Engineering. University of Texas at Austin, MS Thesis, 2006.

[3] Bryant, S., D. Mellor, and C. Cade. Physically Representative Network Models of Transport in Porous Media. *AIChE Journal*, Vol. 39 (1993), No. 3, pp. 387-396.

[4] Al-Raoush, R., K. Thompson, and C.S. Willson. Comparison of Network Generation Techniques for Unconsolidated Porous Media. *Soil Sci. Soc. Am. J*. 67(2003): 1687-1700.

[5] Behseresht, J., S.L. Bryant, and K. Sepehrnoori (2007). Infinite-Acting Physically Representative Networks for Capillarity-Controlled Displacements. SPE 110581 prepared for SPE ATCE 2007, Anaheim, CA, November.

[6] Behseresht, J., Y. Peng, M. Prodanovic, S. Bryant, A. Jain, and R. Juanes. Mechanisms by Which Methane Gas and Methane Hydrate Coexist In Ocean Sediments. OTC19332, Proceedings of the 2008 Offshore Technology Conference, Houston, Texas, U.S.A., 5–8 May, 2008.

[7] Mason, G. and D.W. Mellor. Simulation of Drainage and Imbibition in a Random packing of Equal Spheres. *J. Colloid Interface Sci*. 176 (1995): 214-225.

[8] Mayer, R.P. and R.A. Stowe. Mercury porosimetry-breakthrough pressure for penetration between packed spheres. *J. Colloid Interface Sci*. 20(1965): 893.

[9] Princen, H.M. Capillary phenomena in assemblies of parallel cylinders I. Capillary rise between 2 cylinders. *J. Colloid Interface Sci*. 30 (1969): 69.

[10] Princen, H.M.. Capillary phenomena in assemblies of parallel cylinders II. Capillary rise in systems with more than 2 cylinders. *J. Colloid Interface Sci*. 30 (1969): 359.

[11] Princen, H.M. Capillary phenomena in assemblies of parallel cylinders III. Liquid columns between horizontal parallel cylinders *J. Colloid Interface Sci*. 34 (1970): 171.

[12] Prodanović, M. and S.L. Bryant. A level set method for determining critical curvatures for drainage and imbibition. *J. Colloid Interface Sci*., Vol. 304 (2006), Issue 2, Pages 442-458.

[13] Prodanović, M. and S.L. Bryant. Physics-driven interface modeling for drainage and imbibition in fractures. SPE 110448 prepared for SPE ATCE, Anaheim, CA, November 2007.

[14] Prodanović, M. and S.L. Bryant (2008). Resolving Meniscus Movement Within Rough Confining Surfaces Via the Level Set Method. In *Focus on Water Resource Research Trends,* ed. Eetu Haikkinen, Nova Science Publishers, Hauppage, New York. In press.

[15] Chu, K.T. and M. Prodanović: Level Set Method Library (LSMLIB), http://www.princeton.edu/~ktchu/software/lsmlib/.

[16] Tre´hu, A., P. Flemings, N. Bangs, J. Chevallier, E. Gra`cia, J. Johnson, C.-S. Liu, X. Liu, M. Riedel and M. Torres. Feeding methane vents and gas hydrate deposits at south Hydrate Ridge. *Geophys. Res. Lett.* 31 (2004) L23310, doi:10.1029/2004GL021286.

[17] Torres, M., K. Wallmann, A. Trehu, G. Bohrman, W. Borowski and H. Tomaru. Gas hydrate growth, methane transport, and chloride enrichment at the southern summit of Hydrate Ridge, Cascadia margin off Oregon. *Earth and Planetary Science Letters* 226 (2004), 225–241.

[18] Chen, D. and L. Cathles. A kinetic model for the pattern and amounts of hydrate precipitated grom a gas stream: Appliation to the Bush Hill vent site, Green Canyon Block 185, Gulf of Mexico. *J. Geophys. Res.* 108 (2003, B1) 2058, doi:10.1029/2001JB001597.

[19] Sultan, N., M. Voisset, T. Marsset, A. Vernant, E. Cauquil, J. Colliat and V. Curinier. Detection of free gas and gas hydrate based on 3D seismic data and cone penetration testing: An example from the Nigerian Continental Slope. *Marine Geology* 240 (2007), 235–255.

[20] Milkov, A., G. Dickens, G. Claypool, Y.-J. Lee, W. Borowski, M. Torres, W. Xu, H. Tomaru, A. Trehu and P. Schultheiss. Co-existence of gas hydrate, free gas, and brine within the regional gas hydrate stability zone at Hydrate Ridge (Oregon margin): evidence from prolonged degassing of a pressurized core. *Earth and Planetary Science Letters* 222 (2004), 829–843.

[21] Collett, T.S., R.E. Lewis, S.R. Dallimore, M.W. Lee, T.H. Mroz, and T. Uchida. Detailed evaluation of gas hydrate reservoir properties using JAPEX/JNOC/GSC Mallik 2L-38 gas hydrate research well downhole well-log displays; in *Scientific Results from JAPEX/JNOC/GSC Mallik 2L-38 Gas Hydrate Research Well, Mackenzie Delta, Northwest Territories, Canada*, ed. S. R. Dallimore, T. Uchida and T.S. Collett. *Bull. Geol. Surv. Can.* 544 (1999), 295-311.

[22] Gladkikh, M. and S. Bryant. Prediction of Imbibition from Grain-Scale Interface Movement. *Advances in Water Resources*, Vol. 30 (2007), Issue 2, February, Pages 249-260.